Physics and Imaging in Radiation Oncology 14 (2020) 32–38

Contents lists available at ScienceDirect

Physics and Imaging in Radiation Oncology

journal homepage: www.elsevier.com/locate/phro

Original Research Article

Analytical modeling of depth-dose degradation in heterogeneous lung tissue for intensity-modulated proton therapy planning

Johanna Winter[a,b,c,d,*], Malte Ellerbrock[c,e], Oliver Jäkel[a,c,e], Steffen Greilich[a,c], Mark Bangert[a,c]

[a] Department of Medical Physics in Radiation Oncology, German Cancer Research Center (DKFZ), Im Neuenheimer Feld 280, 69120 Heidelberg, Germany
[b] Department of Physics and Astronomy, Heidelberg University, Heidelberg, Germany
[c] Heidelberg Institute for Radiation Oncology (HIRO), Heidelberg, Germany
[d] Helmholtz Zentrum München GmbH, German Research Center for Environmental Health (HMGU), Institute of Radiation Medicine (IRM), Ingolstädter Landstr. 1, 85764 Neuherberg, Germany
[e] Heidelberg Ion Beam Therapy Center (HIT), Department of Radiation Oncology, Heidelberg University Hospital, Heidelberg, Germany

ARTICLE INFO

Keywords:
Depth-dose degradation
Bragg peak degradation
Proton therapy
Radiotherapy planning
Heterogeneous lung tissue
Non-small-cell lung carcinoma

ABSTRACT

Background and purpose: Proton therapy may be promising for treating non-small-cell lung cancer due to lower doses to the lung and heart, as compared to photon therapy. A reported challenge is degradation, *i.e.*, a smoothing of the depth-dose distribution due to heterogeneous lung tissue. For pencil beams, this causes a distal falloff widening and a peak-to-plateau ratio decrease, not considered in clinical treatment planning systems.
Materials and methods: We present a degradation model implemented into an analytical dose calculation, fully integrated into a treatment planning workflow. Degradation effects were investigated on target dose, distal dose falloffs, and mean lung dose for ten patient cases with varying anatomical characteristics.
Results: For patients with pronounced range straggling (in our study large tumors, or lesions close to the mediastinum), degradation effects were restricted to a maximum decrease in target coverage (D_{95} of the planning target volume) of 1.4%. The median broadening of the distal 80–20% dose falloffs was 0.5 mm at the maximum. For small target volumes deep inside lung tissue, however, the target underdose increased considerably by up to 26%. The mean lung dose was not negatively affected by degradation in any of the investigated cases.
Conclusion: For most cases, dose degradation due to heterogeneous lung tissue did not yield critical organ at risk overdosing or overall target underdosing. However, for small and deep-seated tumors which can only be reached by penetrating lung tissue, we have seen substantial local underdose, which deserves further investigation, also considering other prevalent sources of uncertainty.

1. Introduction

Lung cancer, which is the main cause of cancer-related mortality [1], is commonly treated with concomitant radio-chemotherapy. However, the application of radio-chemotherapy is limited by radiation-induced side effects in organs at risk close to the tumor. Proton therapy can improve overall survival by reducing the dose to the heart and healthy parts of the lung, as compared to photon therapy, due to the inverse depth-dose profile of the Bragg curve [2,3]. This holds true especially for early-stage non-small-cell lung cancer, as well as large primary (diameter greater than 5 cm), centrally located, and recurrent tumors [2,4].

Nevertheless, at present, proton therapy is not widely applied for treatment of lung cancer, which may be attributed to three main challenges: First, internal motion, mainly due to breathing, deteriorates the dose distribution [5–7]. Second, range uncertainties due to setup errors or defective conversion from x-ray computed tomography (CT) numbers to stopping power ratio can lead to underdosing of the tumor and overdosing of organs at risk [7,8]. Third, degradation of the depth dose due to the heterogeneous fine structure in lung tissue yields fluctuation in the water-equivalent thickness over the length of the alveoli, which widens the advantageously sharp distal falloff. For clinical treatment planning systems, this degradation is currently not considered because the alveolar diameter is typically 100–500 μm, which is smaller than the voxel size of clinical CT images (≥ 1 mm^3).

First approaches to account for degradation have been verified with

* Corresponding author at: Helmholtz Zentrum München GmbH, German Research Center for Environmental Health (HMGU), Institute of Radiation Medicine (IRM), Ingolstädter Landstr. 1, 85764 Neuherberg, Germany.
E-mail address: johanna.winter@helmholtz-muenchen.de (J. Winter).

https://doi.org/10.1016/j.phro.2020.05.001
Received 24 February 2020; Received in revised form 2 May 2020; Accepted 7 May 2020

experiments and Monte Carlo simulations of monoenergetic proton beams [9–12]. For a few phantom and patient cases, it was shown that the degradation can lead to underdosing of the tumor and overdosing of organs at risk [11,13–15].

Here, we describe the implementation of a model for dose degradation into an analytical dose calculation engine that is fully integrated into a treatment planning workflow. This enabled a first comprehensive study of the degradation effects in ten clinical cases.

2. Materials and methods

2.1. Model implementation

We used the open-source treatment planning toolkit matRad, which was validated against the clinical syngo RT planning software (Siemens Healthineers, Erlangen, Germany) [16]. MatRad's source code is openly available at http://e0404.github.io/matRad/. MatRad facilitated a pencil-beam algorithm for dose calculation with a Gaussian parameterization of the depth dose. Degradation was implemented in matRad by convolving the pristine Bragg curve, which underlay the dose calculation, with a Gaussian filter. The Gaussian standard deviation σ_{deg} depended on the depth of penetration into lung tissue t_{lung}, which can be computed with matRad's raytracing algorithm, and the modulation power P_{mod}

$$\sigma_{deg} = \sqrt{P_{mod} \bullet t_{lung}}$$

A detailed description of the degradation algorithm is presented in Supplementary Material A.

The modulation power determines the magnitude of the degradation of the Bragg peak as a function of the alveolar diameter and is motivated in detail in Baumann et al. [11]. In agreement with previous publications [9,11,15,17] and consistent with in-house measurements of a lung phantom and a swine lung sample [12], we used a representative value of $P_{mod,rep} = 256$ µm as a most probable scenario. Additionally, the maximum reported modulation power [9] of $P_{mod,max} = 750$ µm served as a worst case scenario.

2.2. Validation

The implementation of our degradation model was verified with in-house shoot-through experiments using proton beam kinetic energies of 100 MeV to 135 MeV and corresponding Monte Carlo simulations [12]. A single Bragg curve was measured twice in a water phantom (pristine curves) and once with a 30-mm slab of lung phantom (Gammex lung 455, Sun Nuclear Corporation, serial no. 45564732, relative electron density 0.30) inserted in front of the water phantom (degraded curve). For each energy, the integral depth-dose curves were normalized by the area under the pristine curves for energy conservation reasons. Both the pristine and the degraded Bragg curves calculated with matRad matched the measurements and Monte Carlo simulations (Fig. 1); the average of the dose difference (relative to the peak) between matRad, measurements, and simulation did not exceed 0.045%.

2.3. Treatment planning

The impact of the degradation was investigated in ten patient cases that were previously treated with photon IMRT at Heidelberg University Hospital1[1] (target volume properties and beam configurations in Table B1 in Supplementary Material B). All patients consented to the anonymous use of their data for research purposes as part of their treatment agreement with Heidelberg University Hospital. Original treatment plans using protons were generated with syngo RT planning based on the PTV without robust optimization. The cases were grouped by tumor size and location:

- Group L: target volumes in the middle of the left or right lung.
- Group C: centrally located tumors, *i.e.*, close to the mediastinum.
- Group W: widespread tumors that covered a large part of the lung (s).

Beams for group L traveled completely through lung tissue, while beams for groups C and W traveled partly through lung tissue, *i.e.*, parts of the tumor were reached by protons that did not undergo degradation. More specifically for group W, beams traveled through lung tissue only within or behind the planning target volume (PTV).

Original DICOM treatment plans and dose distributions from syngo RT planning were imported into matRad on a $(2\ mm)^3$ grid, and then recalculated with the heterogeneity correction turned off ("homogeneous lung") and turned on ("heterogeneous lung"). In either case, pencil-beam grids and intensities from the original treatment plan generated with syngo RT planning were used. The "homogeneous lung" plans were used as reference to account for dose differences arising from heterogeneity only, rather than those arising from different planning systems.

2.4. Dosimetric effects

The recalculated plans were compared by means of transversal dose distributions, absolute dose differences, depth-dose curves, dose-volume histograms (DVHs), quality indicators (QIs) of the clinical target volumes (CTVs) and PTVs for tumor coverage (D_{95}, minimum dose received by 95% of the PTV), and the median dose (D_{50}). As DVHs and QIs did not consider single dose points but were affected by volume averaging, additional contours were added around the PTV, where the strongest degradation effects occurred: The "PTV ring 1" was a 10 mm thick hollow sphere outside of the PTV, while the "PTV ring 2" was a 10 mm thick hollow sphere outside of the "PTV ring 1". For both ring contours, the changes in the mean dose were measured.

To investigate the mean lung dose, the healthy part of the lung was separated from the CTV by "Ipsilateral Lung excluding (w/o) CTV" and "Both Lungs w/o CTV".

According to the International Commission on Radiation Units and Measurements, the target underdose was defined as the subvolume, V_{under}, of the PTV receiving less than 95% of the prescribed dose, thus $V_{under} = V_{PTV} - V_{95}$ [18]. V_{PTV} is the volume of the delineated PTV and V_{95} is the volume within the PTV receiving at least 95% of the prescribed dose.

Two supplemental metrics specific for changes in the spread-out Bragg peak (SOBP) distal dose falloff were applied. The distal falloff, $z_{80\text{-}20}$, measured the water-equivalent distance that the depth-dose curve needed to drop from 80% to 20% of the prescribed dose behind the high-dose plateau of the SOBP. It was calculated along the direction of each pencil beam which reached at least 95% of the prescribed dose.

3. Results

3.1. Target dose

Table 1 provides a comprehensive overview of the QI changes for the target volumes and ring structures. For centrally located and widespread tumors (groups C and W), relative QI changes were less than 0.8%. The largest changes occurred for tumors fully surrounded by lung tissue (group L), where the maximum QI change was 1.6% in PTV ring 1. In all cases, the D_{50} value of the PTV decreased.

An overview of the underdosed volume V_{under} within the PTV in the case of homogeneous lung and its relative increase, $\Delta_{rel}V_{under}$, are given in Table 1. The relative increase of the underdosed volume was smallest for group C (2% at the maximum); for one case, the underdose even

[1] We used eight different patient CT data sets; for two patients, we considered two different beam configurations.

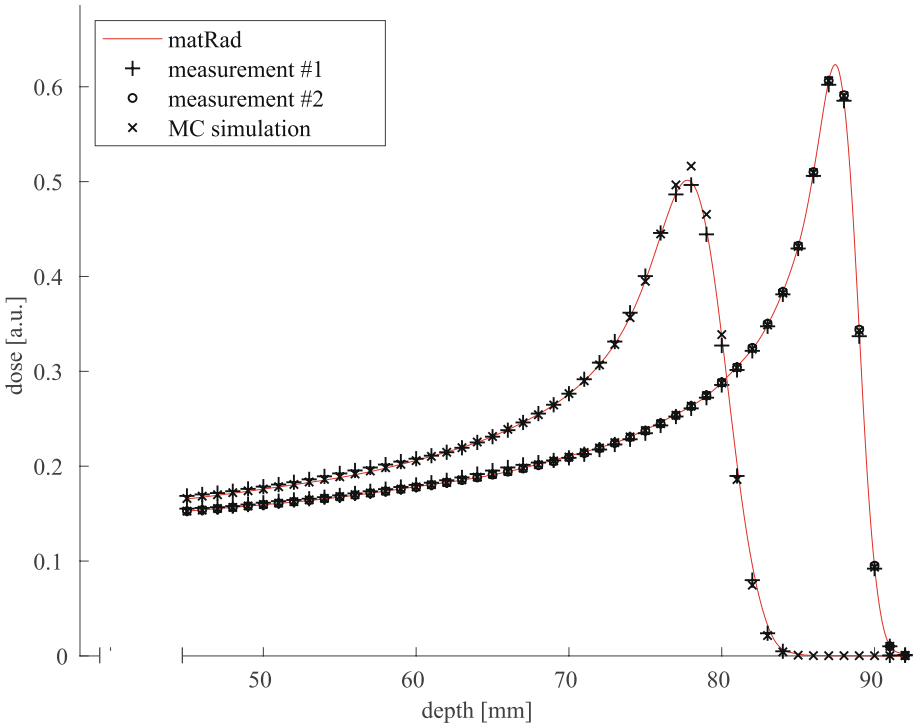

Fig. 1. Model validation. Integrated pristine depth-dose curves for pure water (right peak) and integrated degraded depth-dose curves (left peak) were measured, Monte Carlo (MC)–simulated, and calculated with matRad. The degraded curves were obtained behind a 30 mm-thick lung phantom (Gammex lung 455, Sun Nuclear Corporation, serial no. 45564732). The proton energy was 108.88 MeV. The pristine and degraded depth doses were normalized to the area under the curve for energy conservation.

Table 1
Relative changes in quality indicators of the clinical target volume (CTV), planning target volume (PTV), the ring contours, the underdosed volume, V_{under}, (homogeneous lung), and its relative increase, Δ_{rel} V_{under}, as defined in Section 2.4. Negative values indicate a decrease by introducing degradation, *i.e.*, $\Delta D_X = (D_X \text{ (hetero)} - D_X\text{(homo)})/D_X\text{(homo)}\cdot 100\%$.

Group	Patient ID	CTV ΔD_{95} (%)	PTV ΔD_{95} (%)	PTV ΔD_{50} (%)	PTV ring ΔD_{mean} (%)		V_{under} (%)	Δ_{rel} V_{under} (%)
					ring 1	ring 2		
L	S01	−1.1	−1.3	−1.0	−1.1	−0.7	10.8	20.4
L	S02	−0.7	−1.4	−0.7	−0.8	0.2	15.4	25.3
L	S06	0.3	0.1	−1.5	−1.6	−0.5	20.2	26.2
C	S07_1	0.5	0.3	−0.2	−0.4	−0.4	56.8	1.2
C	S07_2	0.2	0.4	−0.1	−0.5	−0.4	9.3	−7.1
C	S08	−0.1	0.4	−0.1	−0.1	0.0	36.8	1.1
C	S04	−0.1	−0.1	−0.1	−0.2	0.1	28.5	2.1
W	S03_2	−0.1	−0.7	−0.1	−0.3	0.3	6.2	15.1
W	S03_3	−0.2	−0.5	−0.1	−0.2	0.3	8.2	12.4
W	S05	−0.5	−0.8	0.0	−0.1	0.2	15.9	3.8

decreased as cold spots of the inhomogeneous dose distribution were filled up during degradation. For group L, *i.e.*, tumors fully surrounded by lung tissue and PTVs being comparably small (see Table B1 in Supplementary Material B), the underdosed volume increased by 20–26%.

The most pronounced dose changes occurred in patients S06 and S01. An exemplary transversal CT slice of patient S06 with the dose and dose difference overlay is depicted in Fig. 2. It illustrates the broader distal dose falloff along the beam directions with heterogeneity correction turned on. Local dose differences behind the target volume were up to 15% of the prescribed dose.

3.2. Distal falloffs

The distal falloff values, $z_{80\text{-}20}$, as calculated along each pencil beam and their respective median value per treatment field were compared between individual treatment fields among the cases (median values in Table B2 in Supplementary Material B). The median falloff values were between 7 and 64 mm in groups C and W, and between 4 and 9 mm in group L for both the homogeneous and heterogeneous lung.

By applying heterogeneity correction, the median distal falloff did not increase by more than 0.4 mm except for one pencil beam, which increased by 3.8 mm.

For each pencil beam, the absolute change in the distal falloff was associated to the pristine falloff, *i.e.*, to the $z_{80\text{-}20}$ value for the homogeneous lung plan. Small $z_{80\text{-}20}$ values, *i.e.*, steep pristine falloffs, demonstrated a larger increase than larger $z_{80\text{-}20}$ values. This relationship was observed for all proton beams that traveled through the lung tissue. For cases with very large pristine falloff values, *e.g.* due to opposing beams, the beam paths through the lung tissue did not cause a substantial additional widening of the already wide falloffs.

3.3. Dose-volume histograms

Fig. 3 shows the DVHs for cases S08 and S06. S08 is representative for group C with no differences between recalculations with the homogeneous and heterogeneous lung. For case S06, the hot spots of almost 13 Gy (RBE) within the target volumes shrunk upon heterogeneity correction. Changes in D_{50} values were consistent with previous observations. Within the ring contours, the dose was redistributed as the high-dose volume slightly decreased, while the low-dose volume slightly increased. The dose within the lung contours did not change in any DVH.

3.4. Mean lung dose

The mean lung dose within the ipsilateral lung excluding the CTV decreased (up to −1.2%) for all cases. The degraded dose falloff pushed the dose partially from the lung into the tissues behind the lung. The mean dose to both lungs excluding the CTV remained constant or decreased in all but one case (increase by 0.1%). For this case, S03_3, the broader dose falloff of a beam coming from 90° led to a higher dose in the contralateral lung, which outweighed the mean-dose decrease in the ipsilateral lung.

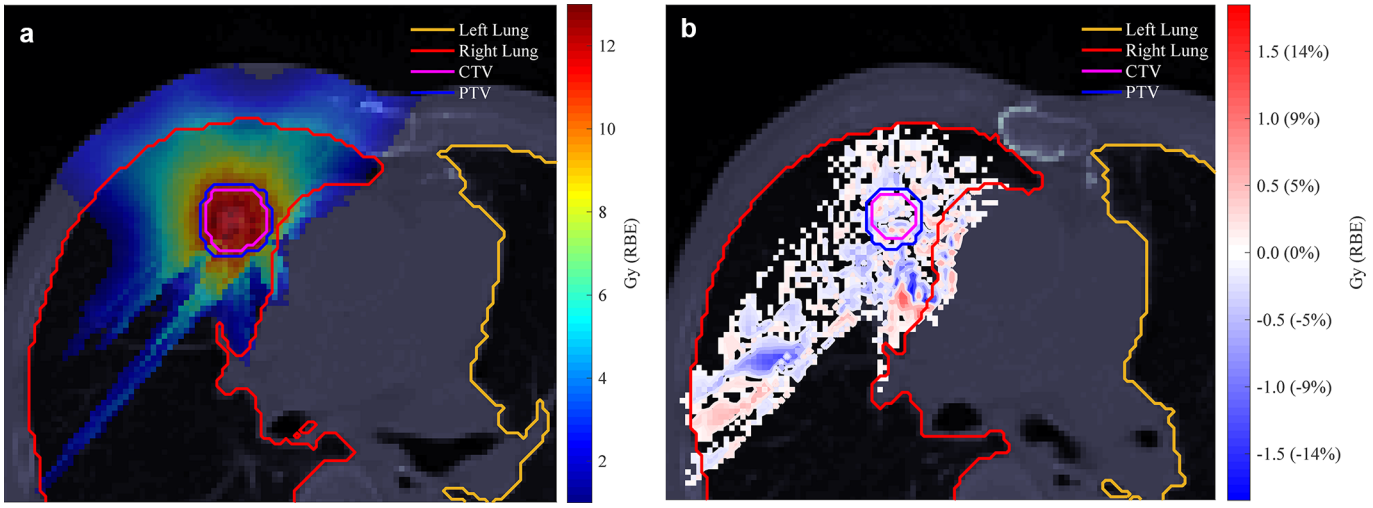

Fig. 2. Two-dimensional dose distribution of patient S06 for homogeneous lung tissue (a) and corresponding dose difference distribution by introducing heterogeneity correction (b). In (b), the blue areas indicate volumes that received lower doses with heterogeneity correction than without. The prescribed dose was 11 Gy (RBE) with the use of three coplanar treatment field orientations (gantry at 40°, 300°, and 340°; couch at 0°).

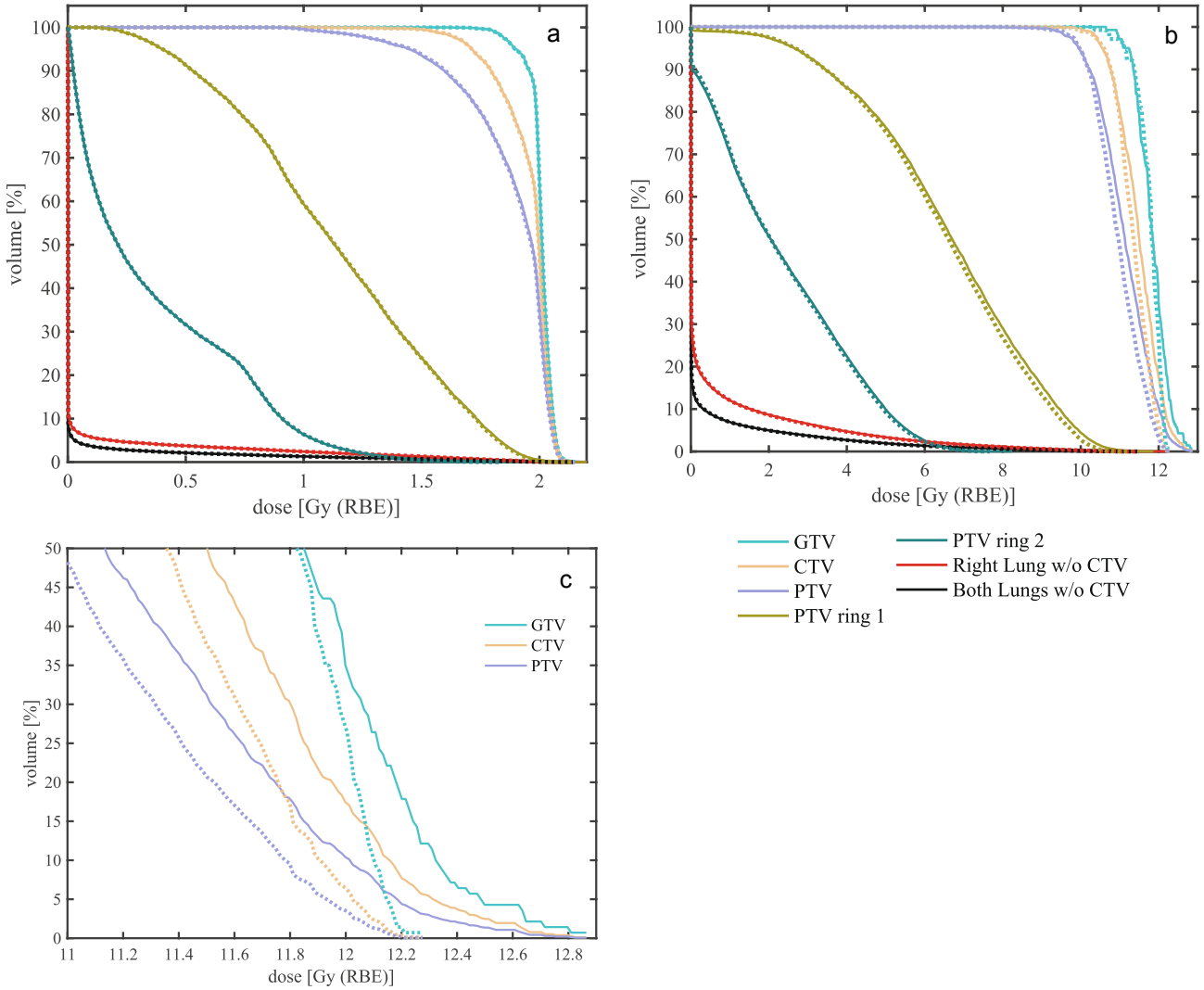

Fig. 3. Dose-volume histograms of patients S08 (a) and S06 (b, c). Histograms for homogeneous lung tissues are indicated by solid lines and histograms for heterogeneous lung tissues by dotted lines. (c) Hot spots in target dose decreased upon heterogeneity correction.

Table 2
Relative changes of quality indicators (QIs) for patient case S06 by introducing degradation with maximum modulation power ($P_{mod,max}$ = 750 µm) and representative modulation power ($P_{mod,rep}$ = 256 µm). For definitions of volumes and QIs, see Section 2.4.

Volume QI	Single voxel Max. dose difference	PTV ΔD_{50}	PTV V_{under} heterogeneous	PTV Δ_{rel} V_{under}	PTV ring 1 ΔD_{mean}	PTV ring 2 ΔD_{mean}
Relative change for $P_{mod,max}$	−27%	−4.4%	44%	119%	−4.9%	−2.2%
Relative change for $P_{mod,rep}$	−23%	−1.5%	25%	26%	−1.6%	−0.5%

3.5. Worst case assessment

The dose distribution in the worst case assessment ($P_{mod,max}$ = 750 µm) showed similar but larger effects than for $P_{mod,rep}$ = 256 µm. Hence, we focused on patient S06 where the degradation had the strongest effect on the dose distribution. Table 2 displays the corresponding QI changes. D_{50} decreased by 4.4% by introducing heterogeneity correction, while maximum dose differences remained comparable to those for $P_{mod,rep}$ = 256 µm. The underdosed target volume increased by 119%. The dose to the lung did not change by applying degradation with the maximum modulation power.

4. Discussion

This is the first comprehensive study investigating the clinical relevance of dose degradation effects in intensity-modulated proton therapy for lung cancer. Our study comprised ten patient cases with large to small tumors located centrally within the thorax or more toward its periphery. In agreement with previous work [10,11,15], the overall effects were moderate, especially for larger tumors where volume averaging effects within the target may compensate negative effects regarding local underdose that may be observed for smaller tumors.

For the ten cases, the dosimetric changes within organs at risk were negligible. As apparent from the PTV ring volume and lung dose analysis, there was no evidence supporting the previously debated overdose to organs at risk close to the tumor [9,11,12,19]. The distal falloffs in our study were in the order of centimeters. Consequently, a median increase of $\Delta z_{80\text{-}20} < 0.5$ mm can be neglected, particularly in consideration of a dose grid resolution of $(2\ mm)^3$.

Phantom simulations, as in Fig. 1, with varying thicknesses of lung tissue demonstrated a noticeable impact of the actual spot modulation resulting from treatment plan optimization on the distal dose falloff. The large impact of optimization of the spot weights and positions on the falloff width is shown in Fig. 4. The position of the last spot of the spread-out Bragg peak relative to the target boundary, which was dependent on the geometrical distance, z_{geo}, of penetrated lung tissue in this experiment, caused variations in the $z_{80\text{-}20}$ value of ± 1 mm. (The geometrical distance z_{geo} refers to the spatial distance that the protons travel through lung as opposed to the water-equivalent distance which accounts for the smaller density of lung tissue.) A high weight on the highest-energy Bragg peak led to a steep pristine distal dose falloff, as seen in Fig. 4b. In contrast, more similar weights on all single Bragg peaks led to a wider pristine dose falloff, as seen in Fig. 4c. Therefore, the median distal falloff increase of less than 0.5 mm when introducing heterogeneity correction is of minor relevance.

For some cases, the mean dose to the “PTV ring 2” increased by up to 0.3%. Nevertheless, there were no organs at risk other than healthy lung located directly behind the target volume in the treatment plans.

We observed a clinically meaningful underdose of the target volume only in patient geometries with small target volumes which can only be reached by penetrating long distances of lung tissue relative to the chest wall.

An increase in the D_{95} value, as observed in four cases (Table 1), is caused by filling up cold spots within the target when the dose distribution is smeared through degradation. A decrease in the D_{95} value can occur when an initially homogeneous dose is degraded and the 95%-isodose is pushed beyond the target boundary.

All simulations were acquired using a pencil-beam dose calculation algorithm, which is still the dominating standard for particle therapy treatment planning. As such, the degradation approach would be applicable not only for intensity-modulated proton therapy but also for passive scattering systems. The general limitations of pencil-beam algorithms within heterogeneous lung tissue, however, are well known and clinical treatment planning for lung cancer should be based on a Monte Carlo dose calculation engine [20,21]. However, in the present study the specific algorithm enabled an isolated investigation of the degradation effects. In addition, we focused on relative effects, rather than the absolute dose values. Therefore, the pencil-beam model does not compromise the overall validity of the conclusions. It may rather be considered as a worst case estimate as pencil-beam dose calculation algorithms generally predict steeper dose gradients within the lung tissue than Monte Carlo dose calculations.

Robust treatment planning could become an important alternative to conventionally optimized plans for proton beam therapy. Robust plans have generally less in-field modulation to compensate for potential mismatches between the geometry during planning and treatment. They are thus more resilient for lung patient treatments [22], which potentially also extends towards degradation.

For a comprehensive clinical assessment, an isolated investigation of the degradation effects may only provide partial guidance. Also, other sources of uncertainty, particularly intrafractional motion [5,7,23], interfractional anatomical changes [24], and setup uncertainties [25] need to be considered, as more severe dosimetric changes are suggested in literature than observed in the context of our study. Many proton centers do not have access to high-quality 3D imaging for patient positioning during treatment which further increases the setup uncertainties for lung tumors [26].

In conclusion, this work presents a comprehensive study of the degradation effects on clinical lung cancer proton treatment plans. For larger and centrally located tumors, the degradation effects were moderate. For small tumors surrounded by lung tissue, however, problems regarding local target underdose might occur. Due to pronounced anatomical variations within lung cancer, our study does not allow for a general recommendation regarding the consideration of degradation effects for clinical practice. Instead, we advocate further research in consideration of other prevalent sources of uncertainty in lung cancer, such as breathing motion or patient setup – especially for small tumor volumes that can only be reached by penetrating substantial amounts of heterogeneous lung tissue. Overall, our study provides promising results as related work has shown that intensity-modulated proton therapy is particularly favorable for large, central, and recurrent tumors, where we see less of a problem for safe clinical application of intensity-modulated proton therapy due to degradation effects.

Declaration of Competing Interest

The authors declare that they have no known competing financial interests or personal relationships that could have appeared to influence the work reported in this paper.

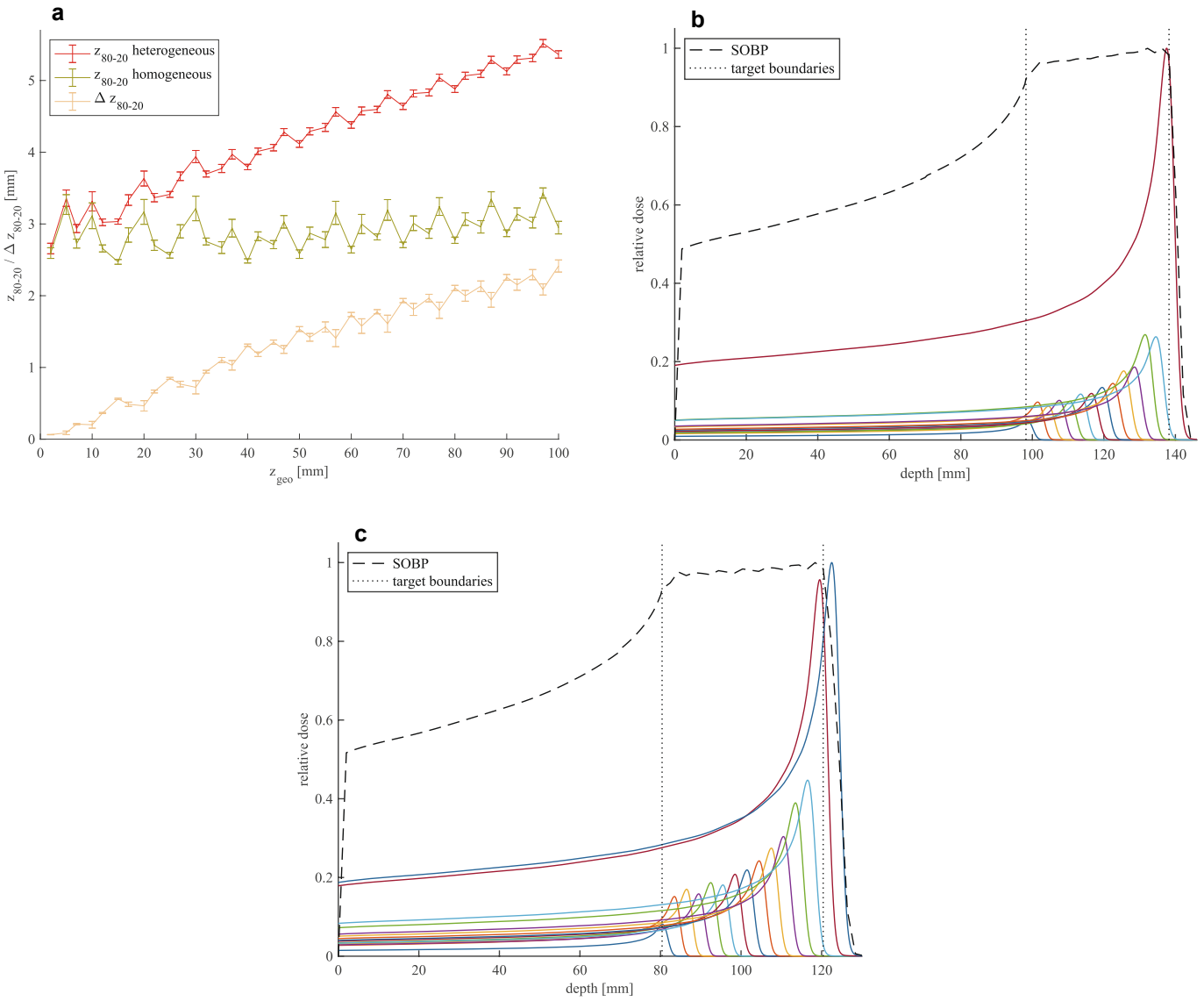

Fig. 4. (a) Distal falloff values, $z_{80\text{-}20}$, of heterogeneous and homogeneous lung tissue, and their difference, $\Delta z_{80\text{-}20}$. The phantom setup was a proton beam impinging on a 30 mm-thick water-equivalent chest wall, a lung-phantom slab (relative electron density 0.30 and variable geometrical distance, z_{geo}), and a water-equivalent cubic target with an edge length of 80 mm. The plans were optimized for homogeneous lung tissue and recalculated with heterogeneity correction on. The mean and standard deviation values of more than 1500 rays are shown. The connection lines are for visual guidance only. (b, c) Different optimizations of the distal end of a spread-out Bragg peak (SOPB). Colored solid lines represent the single Bragg peaks composing the integrated depth dose of the SOBP. A high weight on the highest-energy Bragg peak leads to a steep pristine dose falloff (b), more similar weights on all single Bragg peaks lead to a wider pristine dose falloff (c).

Acknowledgments

We sincerely thank Prof. Dr. Klaus Herfarth and Swantje Ecker from the Heidelberg Ion Beam Therapy Center for providing the patient data.

Funding

This work was supported through the research grant "Intensitätsmodulierte Teilchentherapie für Lungentumore" (70113094) of the German Cancer Aid.

Appendix A + B. Supplementary data

Supplementary data to this article can be found online at https://doi.org/10.1016/j.phro.2020.05.001.

References

[1] Zschaeck S, Simon M, Löck S, Troost EGC, Stützer K, Wohlfahrt P, et al. PRONTOX – proton therapy to reduce acute normal tissue toxicity in locally advanced non-small-cell lung carcinomas (NSCLC): study protocol for a randomised controlled trial. Trials 2016;17:543. https://doi.org/10.1186/s13063-016-1679-4.

[2] Wink KCJ, Roelofs E, Simone CB, Dechambre D, Santiago A, van der Stoep J, et al. Photons, protons or carbon ions for stage I non-small cell lung cancer – Results of the multicentric ROCOCO in silico study. Radiother Oncol 2018;128:139–46. https://doi.org/10.1016/j.radonc.2018.02.024.

[3] Teoh S, Fiorini F, George B, Vallis KA, Van den Heuvel F. Proton vs photon: A model-based approach to patient selection for reduction of cardiac toxicity in locally advanced lung cancer. Radiother Oncol 2019. https://doi.org/10.1016/J.RADONC.2019.06.032.

[4] Chang JY, Jabbour SK, De Ruysscher D, Schild SE, Simone CB, Rengan R, et al. Consensus statement on proton therapy in early-stage and locally advanced non-small cell lung cancer. Int J Radiat Oncol Biol Phys 2016;95:505–16. https://doi.org/10.1016/j.ijrobp.2016.01.036.

[5] Langen K, Jones DT. Organ motion and its management. Int J Radiat Oncol 2001;50:265–78. https://doi.org/10.1016/S0360-3016(01)01453-5.

[6] Knopf A-C, Hong TS, Lomax A. Scanned proton radiotherapy for mobile targets—the effectiveness of re-scanning in the context of different treatment planning

approaches and for different motion characteristics. Phys Med Biol 2011;56:7257–71. https://doi.org/10.1088/0031-9155/56/22/016.
[7] Lin L, Kang M, Huang S, Mayer R, Thomas A, Solberg TD, et al. Beam-specific planning target volumes incorporating 4D CT for pencil beam scanning proton therapy of thoracic tumors. J Appl Clin Med Phys 2015;16:281–92. https://doi.org/10.1120/jacmp.v16i6.5678.
[8] Cho BCJ, van Herk M, Mijnheer BJ, Bartelink H. The effect of set-up uncertainties, contour changes, and tissue inhomogeneities on target dose-volume histograms. Med Phys 2002;29:2305–18. https://doi.org/10.1118/1.1508800.
[9] Witt M. Modulationseffekte von Kohlenstoffionen bei der Bestrahlung von Lungen. Technische Hochschule Mittelhessen (THM) Gießen 2014.
[10] Titt U, Sell M, Unkelbach J, Bangert M, Mirkovic D, Oelfke U, et al. Degradation of proton depth dose distributions attributable to microstructures in lung-equivalent material. Med Phys 2015;42:6425–32. https://doi.org/10.1118/1.4932625.
[11] Baumann K-S, Witt M, Weber U, Engenhart-Cabillic R, Zink K. An efficient method to predict and include Bragg curve degradation due to lung-equivalent materials in Monte Carlo codes by applying a density modulation. Phys Med Biol 2017;62:3997–4016. https://doi.org/10.1088/1361-6560/aa641f.
[12] Dal Bello R. Degradation of proton and carbon Bragg peaks due to density inhomogeneities. Heidelberg, Germany: University of Heidelberg; 2017. https://doi.org/10.11588/heidok.00022822.
[13] Witt M, Weber U, Simeonov Y, Zink K. SU-E-T-671: Range-Modulation Effects of Carbon Ion Beams in Lung Tissue. Med Phys 2015;42:3491. https://doi.org/10.1118/1.4925034.
[14] Baumann K-S, Flatten V, Weber U, Engenhart-Cabillic R, Zink K. EP-1902: analysing the effects of Bragg curve degradation due to lung parenchyma in treatment planning. Radiother Oncol 2018;127:S1031. https://doi.org/10.1016/S0167-8140(18)32211-4.
[15] Flatten V, Baumann K-S, Weber U, Engenhart-Cabillic R, Zink K. Quantification of the dependencies of the Bragg peak degradation due to lung tissue in proton therapy on a CT-based lung tumor phantom. Phys Med Biol 2019. https://doi.org/10.1088/1361-6560/ab2611.
[16] Wieser H-P, Cisternas E, Wahl N, Ulrich S, Stadler A, Mescher H, et al. Development of the open-source dose calculation and optimization toolkit matRad. Med Phys 2017;44:2556–68. https://doi.org/10.1002/mp.12251.
[17] Ringbæk TP, Simeonov Y, Witt M, Engenhart-Cabillic R, Kraft G, Zink K, et al. Modulation power of porous materials and usage as ripple filter in particle therapy. Phys Med Biol 2017;62:2892–909. https://doi.org/10.1088/1361-6560/aa5c28.
[18] Landberg T, Chavaudra J, Dobbs J, Gerard J-P, Hanks G, Horiot J-C, et al. ICRU Report 62: Prescribing, Recording and Reporting Photon Beam Therapy. J Int Comm Radiat Units Meas 1999;os32(1). https://doi.org/10.1093/jicru/os32.1.Report62.
[19] Sawakuchi GO, Titt U, Mirkovic D, Mohan R. Density heterogeneities and the influence of multiple Coulomb and nuclear scatterings on the Bragg peak distal edge of proton therapy beams. Phys Med Biol 2008;53:4605–19. https://doi.org/10.1088/0031-9155/53/17/010.
[20] Taylor PA, Kry SF, Followill DS. Pencil beam algorithms are unsuitable for proton dose calculations in lung. Int J Radiat Oncol Biol Phys 2017;99:750–6. https://doi.org/10.1016/j.ijrobp.2017.06.003.
[21] Maes D, Saini J, Zeng J, Rengan R, Wong T, Bowen SR. Advanced proton beam dosimetry part II: Monte Carlo vs. pencil beam-based planning for lung cancer. Transl Lung Cancer Res 2018;7:114–21. https://doi.org/10.21037/tlcr.2018.04.04.
[22] Inoue T, Widder J, van Dijk LV, Takegawa H, Koizumi M, Takashina M, et al. Limited impact of setup and range uncertainties, breathing motion, and interplay effects in robustly optimized intensity modulated proton therapy for stage III non-small cell lung cancer. Int J Radiat Oncol Biol Phys 2016;96:661–9. https://doi.org/10.1016/j.ijrobp.2016.06.2454.
[23] De Ruysscher D, Sterpin E, Haustermans K, Depuydt T. Tumour movement in proton therapy: solutions and remaining questions: a review. Cancers (Basel) 2015;7:1143–53. https://doi.org/10.3390/cancers7030829.
[24] Hoffmann L, Alber M, Jensen MF, Holt MI, Møller DS. Adaptation is mandatory for intensity modulated proton therapy of advanced lung cancer to ensure target coverage. Radiother Oncol 2017;122:400–5. https://doi.org/10.1016/J.RADONC.2016.12.018.
[25] Paganetti H. Range uncertainties in proton therapy and the role of Monte Carlo simulations. Phys Med Biol 2012;57:R99–117. https://doi.org/10.1088/0031-9155/57/11/R99.
[26] Landry G, Hua C. Current state and future applications of radiological image guidance for particle therapy. Med Phys 2018;45:e1086–95. https://doi.org/10.1002/mp.12744.